

# THE ROLE OF ICE COMPOSITIONS AND MORPHOLOGY FOR SNOWLINES AND THE C/N/O RATIOS IN ACTIVE DISKS

ANA-MARIA A. PISO<sup>1</sup>, KARIN I. ÖBERG<sup>1</sup>, JAMILA PEGUES<sup>2</sup>

*Draft version March 3, 2016*

## ABSTRACT

The elemental compositions of planets define their chemistry, and could potentially be used as beacons for their formation location if the elemental gas and grain ratios of planet birth environments, i.e. protoplanetary disks, are well understood. In disks, the ratios of volatile elements, such as C/O and N/O, are regulated by the abundance of the main C, N, O carriers, their ice binding environment, and the presence of snowlines of major volatiles at different distances from the central star. We explore the effects of dynamical processes, molecular compositions and abundances, and the ice morphology of dust grains in disks on the snowline locations of the main C, O and N carriers, and their consequences for the C/N/O ratios in gas and dust throughout the disk. We find that if CO and N<sub>2</sub> are water dominated instead of pure ices, their snowlines move inward by  $\sim 70\%$ . Both ice morphology and disk dynamics substantially change the disk regions where gas phase C/O and N/O are enhanced over the stellar value, and taken together they may move the CO and N<sub>2</sub> snowlines by a factor of  $\sim 7$  inward. Between the CO<sub>2</sub> and CO snowlines, the gaseous C/O and N/O are enhanced by factors of  $\sim 2$  and  $\sim 3$ , respectively. The gas-phase N/O ratio is enhanced by many orders of magnitude between the CO and N<sub>2</sub> snowlines due to the depletion of oxygen gas in this region. Our estimates for the C/N/O ratios are moderately affected by the presence of some C in the form of CH<sub>4</sub> and of some N in the form of NH<sub>3</sub>.

## 1. INTRODUCTION

The chemical composition of protoplanetary disks is largely dictated by the freeze-out of volatile species. The snowline locations of volatile molecules are therefore crucial in determining disk chemical abundances in gas and dust, as well as planet compositions.

Carbon and oxygen bearing molecules, such as H<sub>2</sub>O, CO<sub>2</sub> and CO, as well as the carbon-to-oxygen (C/O) ratio in protoplanetary disks and in giant planet atmospheres have been extensively studied from a theoretical standpoint (Öberg et al. 2011b, Ali-Dib et al. 2014, Madhusudhan et al. 2014, Mollière et al. 2015), and snowlines of volatiles such as H<sub>2</sub>O and CO have been detected (Zhang et al. 2013, Qi et al. 2013). However, disk chemistry is complex, and it involves many other molecular compounds (Henning & Semenov 2013). In particular, several other volatiles have been detected in disks, such as nitrogen bearing species and hydrocarbons (e.g., Mandell et al. 2012), which adds further complexity to the disk composition.

Both in Solar system comets and in protoplanetary disks carbon and oxygen are primarily contained in H<sub>2</sub>O, CO<sub>2</sub> and CO (e.g., Rodgers & Charnley 2002, Lodders 2003, Pontoppidan 2006). However, some fraction of the carbon abundance may also be carried by CH<sub>4</sub> (e.g., Mumma et al. 1996), which may change the C/O ratio in gas and in dust throughout the disk. Nitrogen is another abundant volatile in the Solar system and in disks. Chemical models of the protostellar nebula (e.g., Owen et al. 2001) and of protoplanetary disks (e.g., Rodgers & Charnley 2002) suggest that N<sub>2</sub> was the dominant form of nitrogen, and that giant planets have ac-

creted their nitrogen content primarily as N<sub>2</sub> (Mousis et al. 2014). Observations of Solar system bodies such as Titan and Pluto show that N<sub>2</sub> is prevalent in their atmospheres (Cruikshank et al. 1993, Owen et al. 1993). Moreover, the Rosetta spacecraft has recently made the first direct measurement of the N<sub>2</sub> abundance in comet 67P/Churyumov-Gerasimenko (Rubin et al. 2015). In addition to N<sub>2</sub>, a fraction of the nitrogen abundances may be also carried by NH<sub>3</sub> (Bottinelli et al. 2010, Mumma & Charnley 2011). Because of the high volatility of N<sub>2</sub>, the gas phase nitrogen-to-oxygen (N/O) ratio in the outer disk may be even more enhanced than the C/O ratio compared to its average value in the disk. Giant planets that form at wide separations should thus have an excess of nitrogen in their atmospheres, which could be used to trace their formation origin.

Moreover, snowline locations strongly depend on the ice grain morphology. Laboratory experiments (Collings et al. 2003, Öberg et al. 2005, Bisschop et al. 2006, Fayolle et al. 2016) have shown that volatiles such as CO and N<sub>2</sub> have significantly different binding energies depending on whether they are pure or water dominated ices. This implies that ices in different environments will sublime at different radii, which will substantially change the disk regions where these volatiles are present in gaseous or solid form (see Section 3.2).

In order to explain this added chemical and physical complexity, a more thorough theoretical framework is needed. In this work, we expand the coupled drift-desorption model developed in Piso et al. (2015) (hereafter Paper I) by considering additional volatile molecules and abundances, ice morphology, as well as nitrogen-to-oxygen (N/O) and nitrogen-to-carbon (N/C) ratios.

This paper is organized as follows. In Section 2, we

<sup>1</sup> Harvard-Smithsonian Center for Astrophysics, 60 Garden Street, Cambridge, MA 02138

<sup>2</sup> Department of Astrophysical Sciences, Princeton University

review the drift-desorption model developed in Paper I. We discuss the effect of different abundances of the main carbon, oxygen and nitrogen carriers, grain morphology and disk dynamics on snowline locations and the C/N/O ratios in Section 3. We discuss the implications of our results in Section 4 and summarize our findings in Section 5.

## 2. COUPLED DRIFT-DESORPTION MODEL

We begin with a brief review of Paper I’s model for the effect of radial drift and viscous gas accretion on volatile snowline locations. We review our disk model in Section 2.1, and summarize our numerical method and results in Section 2.2.

### 2.1. Disk Model

In this work we consider both a static and a viscous disk. The static disk is irradiated by the central star and does not experience redistribution of solids or radial movement of the nebular gas. To quantify the effects of radial drift and gas accretion, we use a viscous disk with a spatially and temporally constant mass flux,  $\dot{M}$ . The viscous disk takes into account radial drift, gas accretion onto the central star, as well as accretion heating. We focus on this disk model which includes all the dynamical and thermal processes we are interested in for the scope of this paper, and do not further consider the other disk models presented in Paper I.

Following Chiang & Youdin (2010), the temperature profile for a static disk is

$$T = 120 (r/\text{AU})^{-3/7} \text{ K}, \quad (1)$$

where  $r$  is the semimajor axis. We use the Shakura & Sunyaev (1973) steady-state disk solution to model the viscous disk. From Paper I, the viscous disk temperature profile is computed as

$$T^4 = \left[ \frac{1}{4r} \left( \frac{3G\kappa_0 \dot{M}^2 M_* \mu m_p \Omega_k}{\pi^2 \alpha k_B \sigma} \right)^{1/3} \right]^4 + T_{\text{irr}}^4, \quad (2)$$

where  $T_{\text{irr}} = T$  from Equation (1). Here  $G$  is the gravitational constant,  $\kappa_0 = 2 \times 10^{-6}$  is a dimensionless opacity coefficient,  $M_* = M_\odot$  is the mass of the central star,  $\mu = 2.35$  is the mean molecular weight of the nebular gas,  $m_p$  is the proton mass,  $\Omega_k = \sqrt{GM_\odot/r^3}$  is the Keplerian angular velocity,  $\alpha = 0.01$  is a dimensionless coefficient (see below for details),  $k_B$  is the Boltzmann constant, and  $\sigma$  is the Stefan-Boltzmann constant.

The steady-state disk has an  $\alpha$ -viscosity prescription, where the kinematic viscosity is  $\nu = \alpha c H$ . Here  $c \equiv \sqrt{k_B T / (\mu m_p)}$  is the isothermal sound speed (with  $T$  from Equation 2), and  $H \equiv c / \Omega_k$  is the disk scale height. We can then determine the gas surface density for a viscous disk as (Shakura & Sunyaev 1973; see also Paper I for a more detailed explanation of these calculations):

$$\Sigma = \frac{\dot{M}}{3\pi\nu}. \quad (3)$$

We choose  $\dot{M} = 10^{-8} M_\odot \text{ yr}^{-1}$ , consistent with mass flux observations in disks (e.g., Andrews et al. 2010). As described in Paper I, the mass flux rate  $\dot{M}$  and stellar luminosity  $L_*$  will vary throughout the disk lifetime

(Kennedy et al. 2006, Chambers 2009), in contrast with our simplified model which assumes that both quantities are constant. This effect will be most pronounced in the inner disk ( $\lesssim$  few AU), where accretion heating dominates. We thus acknowledge that the location of the  $\text{H}_2\text{O}$  snowline may be determined by the decline in  $\dot{M}$  or  $L_*$  with time, rather than radial drift (see Paper I, Section 2.1 for a more detailed explanation).

### 2.2. Desorption-Drift Equations and Results

The model is described in full in Paper I, here we review and summarize key concepts and results. For a range of initial icy grain sizes composed of a single volatile, we showed in Paper I that the timescale on which these particles desorb is comparable to their radial drift time, as well as to the accretion timescale of the nebular gas onto the central star. We thus have to take into account both drift and gas accretion when we calculate the disk location at which a particle desorbs, since that location may be different from the snowline position in a static disk for a given volatile (see Figure 1 and Öberg et al. 2011b). We determine a particle’s final location in the disk by solving the following coupled differential equations:

$$\frac{ds}{dt} = -\frac{3\mu_x m_p}{\rho_s} N_x R_{\text{des},x} \quad (4a)$$

$$\frac{dr}{dt} = \dot{r}, \quad (4b)$$

where  $s$  is the particle size,  $t$  is time,  $\mu_x$  is the mean molecular weight of volatile  $x$ ,  $\rho_s = 2 \text{ g cm}^{-3}$  is the density of an icy particle,  $N_x \approx 10^{15} \text{ sites cm}^{-2}$  is the number of adsorption sites of molecule  $x$  per  $\text{cm}^{-2}$ ,  $R_{\text{des},x}$  is the desorption rate of species  $x$ , and  $\dot{r}$  is the particle’s radial drift velocity. We calculate  $R_{\text{des}}$  and  $\dot{r}$  as follows.

The desorption rate  $R_{\text{des},x}$  (per molecule) is (Hollenbach et al. 2009)

$$R_{\text{des},x} = \nu_x \exp(-E_x/T_{\text{grain}}), \quad (5)$$

where  $E_x$  is the adsorption binding energy in units of Kelvin,  $T_{\text{grain}} = T$  is the grain temperature (assumed to be the same as the disk temperature, see Paper I), and  $\nu_x = 1.6 \times 10^{11} \sqrt{(E_x/\mu_x)} \text{ s}^{-1}$  is the molecule’s vibrational frequency in the surface potential well. We discuss our choices for  $E_x$  for the different volatile species in Sections ?? and ??.

Following Chiang & Youdin (2010) and Birnstiel et al. (2012), a particle’s radial drift velocity can be approximated as

$$\dot{r} \approx -2\eta\Omega_k r \left( \frac{\tau_s}{1 + \tau_s^2} \right) + \frac{\dot{r}_{\text{gas}}}{1 + \tau_s^2}, \quad (6)$$

where the first term is the drift velocity in a non-accreting disk and the second term accounts for the radial movement of the gas. Here  $\eta \approx c^2/(2v_k^2)$ , where  $v_k$  is the Keplerian velocity, and  $\tau_s \equiv \Omega_k t_s$  is the dimensionless stopping time:

$$t_s = \begin{cases} \rho_s s / (\rho c), & s < 9\lambda/4 \text{ Epstein drag} \\ 4\rho_s s^2 / (9\rho c \lambda), & s < 9\lambda/4, \text{Re} \lesssim 1 \text{ Stokes drag,} \end{cases} \quad (7)$$

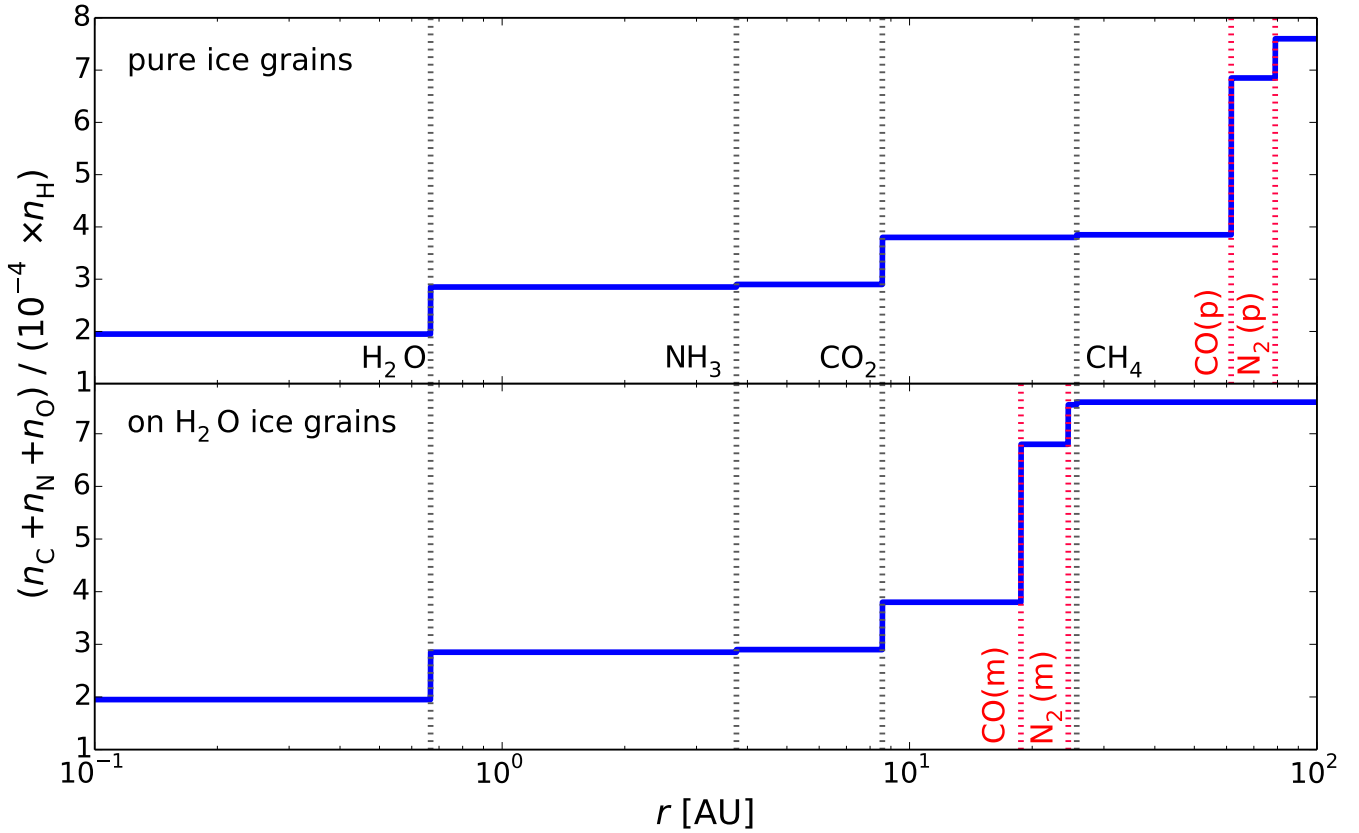


FIG. 1.— The total carbon, nitrogen and oxygen abundance as a function of semimajor axis in a static disk, for CO and N<sub>2</sub> as pure ices (top panel) and water dominated ices (bottom panel). Relevant volatile snowlines are marked by the vertical dashed lines. The grain abundances are calculated as a function of the observed median CH<sub>4</sub> and NH<sub>3</sub> abundances in protostellar cores (see Sections ?? and ??). The total grain abundance increases with semimajor axis as more and more species freeze out.

where  $\rho$  is the disk mid-plane density,  $\lambda$  is the mean free path and  $Re$  is the Reynolds number. The gas accretion velocity  $\dot{r}_{\text{gas}}$  is determined from  $\dot{M} = -2\pi r \dot{r}_{\text{gas}} \Sigma$ , for a fixed  $\dot{M}$  and with  $\Sigma$  given by Equation (3).

For a particle of initial size  $s_0$ , we solve the Equation set (4) with the initial conditions  $s(t_0) = s_0$  and  $r(t_0) = r_0$ , where  $t_0$  is the time at which we start the integration and  $r_0$  is the particle's initial location. We stop our simulation after  $t_d = 3$  Myr, the disk lifetime, since this is roughly the timescale on which planets form, and determine the desorption timescale  $t_{\text{des}}$  from  $s(t_{\text{des}}) = 0$ , and thus a particle's desorption distance  $r_{\text{des}} = r(t_{\text{des}})$ . Our results are insensitive to our choice of  $t_0$  as long as  $t_0 \ll t_d$ . We note that a particle's size is initially fixed and only changes due to desorption. We thus do not take into account processes such as grain coagulation or fragmentation, which nonetheless occur in disks (e.g., Birnstiel et al. 2012, Pérez et al. 2012). We discuss the effect of these processes on snowline locations in Paper I.

As we show in Paper I, a particle of initial size  $s_0$  can experience three outcomes after  $t_d = 3$  Myr: (1) it can remain at its initial location, (2) it can drift towards the host star, then stop without evaporating significantly, and (3) it can completely desorb on a timescale shorter than 3 Myr. Particles in scenarios (1) and (2) are thus not affected by radial drift or gas accretion, and the snow-

line locations are those for a static disk. In contrast, the grains in case (3) desorb practically *instantaneously* and *at a fixed particle-size dependent location* in the disk, regardless of their initial position. The snowline locations for these particles will thus be fixed for a given initial particle size and disk model. We have found that grains with sizes  $\sim 0.001 \text{ cm} \lesssim s \lesssim 7 \text{ m}$  satisfy this condition for our fiducial disk.

### 3. RESULTS

#### 3.1. Snowlines in a Static Disk: The Importance of Ice Morphology

As we note in Section 1, the disk volatile composition and the ice morphology determine the location of several important snowlines. In this work we focus on the primary carbon, oxygen and nitrogen carriers, i.e. H<sub>2</sub>O, CO<sub>2</sub>, CO, N<sub>2</sub>, and to a lesser extent, CH<sub>4</sub> and NH<sub>3</sub>. To qualify the effect of the presence of some carbon in the form of CH<sub>4</sub>, we use measured CH<sub>4</sub> abundances in protostellar cores from the *Spitzer* c2d Legacy ice survey (Evans et al. 2003). We explore the parameter space of possible CH<sub>4</sub> abundances by assuming three different scenarios: (1) no CH<sub>4</sub>, (2) the median CH<sub>4</sub> observed abundance (hereafter CH<sub>4</sub>-mid), and (3) the maximum CH<sub>4</sub> observed abundance (hereafter CH<sub>4</sub>-max). Thus  $n_{\text{CH}_4\text{-mid}} = 0.0555 \times n_{\text{H}_2\text{O}}$  (Öberg et al. 2011a) and  $n_{\text{CH}_4\text{-max}} = 0.13 \times n_{\text{H}_2\text{O}}$  (Öberg et al. 2008), where

$n_{\text{H}_2\text{O}}$  is the total  $\text{H}_2\text{O}$  abundance. Similarly to Paper I, we use the  $\text{H}_2\text{O}$ ,  $\text{CO}_2$  and  $\text{CO}$  abundances of Öberg et al. (2011b). Since the abundance of carbon grains is uncertain, we assume that all the carbon that is not in the form of  $\text{CH}_4$ ,  $\text{CO}$  and  $\text{CO}_2$  is in carbon grains, so that we reproduce the Solar C/O ratio (gas+dust) of 0.54.

We assume that the main nitrogen-bearing species are  $\text{N}_2$  and  $\text{NH}_3$ , since other volatiles that contain nitrogen have significantly lower abundances in comparison (e.g., Mumma & Charnley 2011). We use the measured total nitrogen abundance in the Solar system,  $n_{\text{N}} = 8 \times 10^{-5} n_{\text{H}}$  (Lodders 2003), where  $n_{\text{H}}$  is the hydrogen abundance in the disk midplane. Similarly to the case of  $\text{CH}_4$ , we explore the parameter space of possible  $\text{NH}_3$  abundances using data from the Spitzer c2d Legacy ice survey, as follows: (1) no  $\text{NH}_3$ , (2) the median  $\text{NH}_3$  observed abundance  $n_{\text{NH}_3\text{-mid}} = 0.055 \times n_{\text{H}_2\text{O}}$  (Öberg et al. 2011a), and (3) the maximum observed  $\text{NH}_3$  abundance  $n_{\text{NH}_3\text{-max}} = 0.1537 \times n_{\text{H}_2\text{O}}$  (Bottinelli et al. 2010). In each case, the  $\text{N}_2$  abundance then simply follows as  $n_{\text{N}_2} = (n_{\text{N}} - n_{\text{NH}_3})/2$ .

We determine the location of the  $\text{H}_2\text{O}$ ,  $\text{CO}_2$ ,  $\text{CO}$ ,  $\text{CH}_4$ ,  $\text{N}_2$  and  $\text{NH}_3$  snowlines in our static disk by balancing desorption with readsorption, following Hollenbach et al. (2009). The binding energies of  $\text{H}_2\text{O}$ ,  $\text{CO}_2$ ,  $\text{CO}$ ,  $\text{CH}_4$ ,  $\text{N}_2$  and  $\text{NH}_3$  as pure ices are 5800 K, 2000 K, 834 K, 1300 K, 767 K and 2965 K, respectively (Fraser et al. 2001, Collings et al. 2004, Fayolle et al. 2016, Garrod & Herbst 2006, Martín-Doménech et al. 2014). For  $\text{CO}$  and  $\text{N}_2$  as water dominated ices the binding energies are 1388 K and 1266 K, respectively (Fayolle et al. 2016). Figure 1 shows the resulting snowline locations, with  $\text{CO}$  and  $\text{N}_2$  pure ices (top panel) and water dominated ices (bottom panel). The ordinate displays the total carbon, oxygen and nitrogen abundance in solids as a function of the hydrogen total abundance. We assume that the  $\text{CH}_4$  and  $\text{NH}_3$  abundances are  $n_{\text{CH}_4\text{-mid}}$  and  $n_{\text{NH}_3\text{-mid}}$ . As expected, the total grain abundance increases with semimajor axis, as more and more species sublime. More importantly, the  $\text{CO}$  and  $\text{N}_2$  snowlines move several tens of AU inward if the ices are water dominated rather than pure. This changes the chemical abundances both in gas and dust throughout the disk, directly affecting the compositions of nascent giant planets forming in situ.

### 3.2. C/N/O Ratios in Static Disks

In this section we determine the C/O and N/O ratios in gas and dust throughout our static disk, and the extent by which they are affected by the presence of  $\text{CH}_4$  and  $\text{NH}_3$ . Since here we are primarily interested in the magnitude of the C/N/O ratios rather than snowline locations (which have been discussed extensively in Section 3.1), we assume for simplicity that  $\text{CO}$  and  $\text{N}_2$  are pure ices.

Figure 2 shows the C/O ratio in gas and dust as a function of semimajor axis in a static disk, for three different  $\text{CH}_4$  abundances as outlined above: no  $\text{CH}_4$  (top panel),  $\text{CH}_4\text{-mid}$  (middle panel) and  $\text{CH}_4\text{-max}$  (bottom panel). As in Öberg et al. (2011b) and Paper I, a gaseous C/O ratio of unity can be achieved between the  $\text{CO}_2$  and  $\text{CO}$  snowlines, where oxygen gas is significantly depleted. The gas-phase C/O ratio may be further enhanced between the  $\text{CO}_2$  and  $\text{CH}_4$  snowlines due to the presence

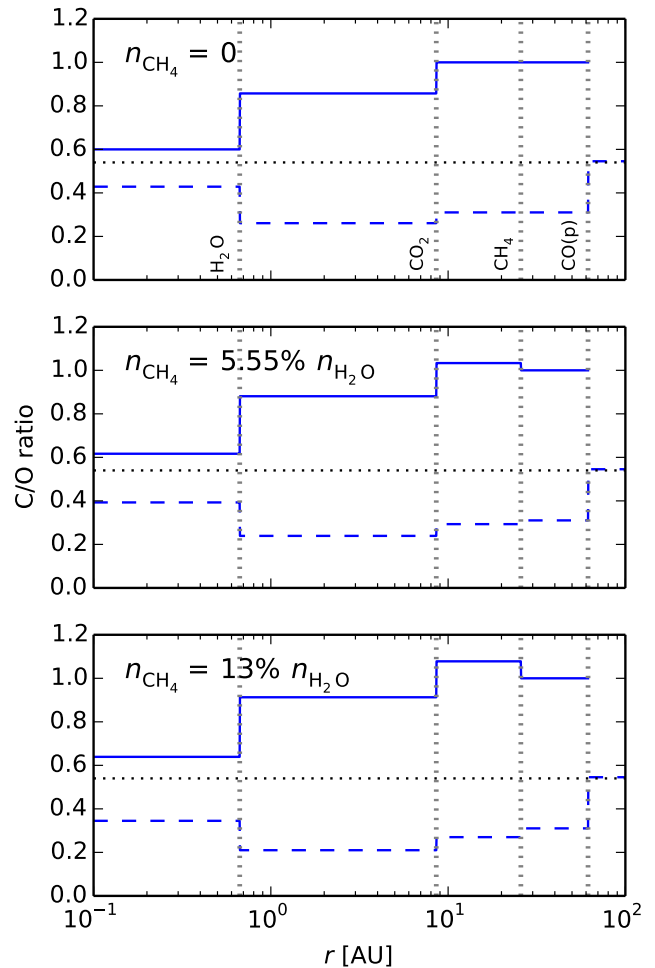


FIG. 2.— The C/O ratio in gas (solid lines) and dust (dashed lines) as a function of semimajor axis in a static disk, assuming no carbon is present in the form of  $\text{CH}_4$  (top panel), the median observed  $\text{CH}_4$  abundance is assumed (middle panel), and the maximum observed  $\text{CH}_4$  abundance is assumed (bottom panel). The C/O estimates are performed assuming that the  $\text{CO}$  ices are in pure form. The vertical dashed lines mark the snowline locations of the main C and O carriers. The horizontal dashed lines represent the stellar C/O value. The presence of methane only modestly increases the C/O ratio in gas between the  $\text{CO}_2$  and  $\text{CH}_4$  snowlines.

of additional carbon gas from  $\text{CH}_4$ . In this region, the C/O ratio increases by 3% for  $\text{CH}_4\text{-mid}$  and by 8% for  $\text{CH}_4\text{-max}$ , as displayed in the middle and bottom panels of Figure 2. Based on the range of observed  $\text{CH}_4$  protostellar abundances, its presence in the disk only modestly affects the C/O ratio. Given the larger uncertainties in overall volatile abundances, we can neglect  $\text{CH}_4$  when estimating the C/O ratio in disks.

Figure 3 shows the snowline locations of the main oxygen and nitrogen carriers and the N/O ratio in gas and dust as a function of semimajor axis in a static disk, for our three choices of the  $\text{NH}_3$  abundance (see Section 3.1): no  $\text{NH}_3$  (top panel),  $\text{NH}_3\text{-mid}$  (middle panel) and  $\text{NH}_3\text{-max}$  (bottom panel). For comparison, the horizontal dashed lines show the average N/O ratio in the disk. As expected, the gaseous N/O ratio generally exhibits an increasing trend towards the outer disk as more oxygen gas is depleted, with small decreases between the

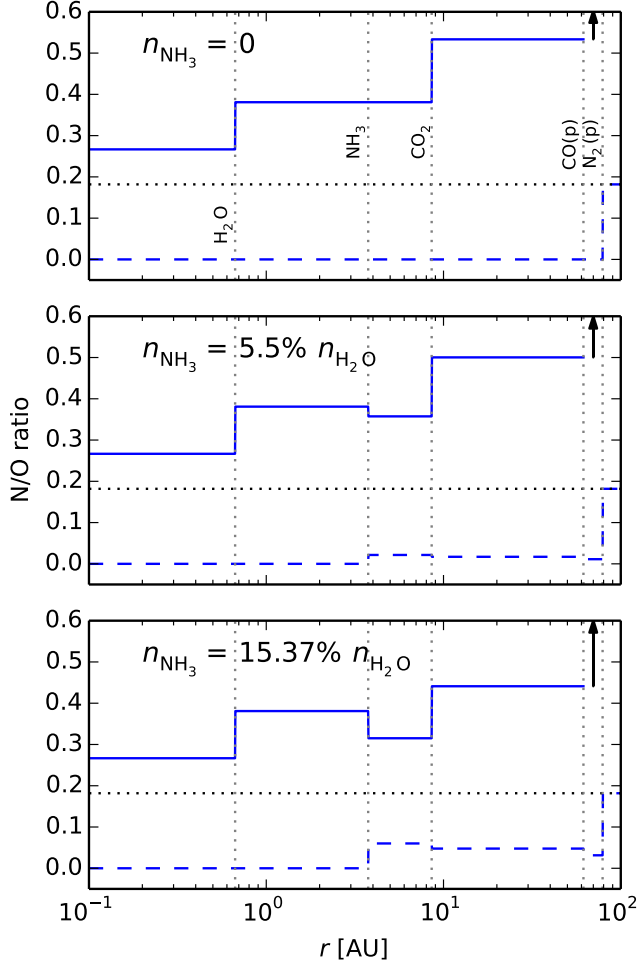


FIG. 3.— The N/O ratio in gas (solid lines) and dust (dashed lines) as a function of semimajor axis in a static disk, assuming no nitrogen is present in the form of  $\text{NH}_3$  (top panel), the median observed  $\text{NH}_3$  abundance is assumed (middle panel), and the maximum observed  $\text{NH}_3$  abundance is assumed (bottom panel). The N/O estimates are performed assuming that the CO and  $\text{N}_2$  ices are in pure form. The vertical dashed lines mark the snowline locations of the main C,O and N carriers. The horizontal dashed lines represent the average N/O value in the disk. The gas-phase N/O ratio is highly enhanced in the outer disk (by more than a factor of three) compared to its average value. The arrows mark a highly elevated N/O ratio in gas between the CO and  $\text{N}_2$  snowlines due to the depletion of oxygen gas in this region. The presence of  $\text{NH}_3$  moderately decreases the N/O ratio in gas between the  $\text{NH}_3$  and  $\text{CO}_2$  snowlines.

$\text{NH}_3$  and  $\text{CO}_2$  snowlines (by 16% for  $\text{NH}_3$ -mid and by 18% for  $\text{NH}_3$ -max, respectively) due to  $\text{NH}_3$  freeze-out. While the presence of  $\text{NH}_3$  only moderately affects our results for the N/O ratio,  $\text{NH}_3$  is important since otherwise there would be no solid nitrogen inside the  $\text{N}_2$  snowline, which would be contrary to asteroid and comet observations (Wyckoff et al. 1991, Mumma & Charnley 2011, Bergin et al. 2015).

The gas-phase N/O ratio is enhanced by a factor of two outside the  $\text{H}_2\text{O}$  snowline compared to its average value, by more than a factor of three between the  $\text{CO}_2$  and CO snowlines, and by orders of magnitude between the CO and  $\text{N}_2$  snowlines, which can span tens of AU depending on disk parameters and the relative CO and

$\text{N}_2$  ice binding environment. This enhancement is more pronounced than the C/O gas-phase enhancement of a factor of two in the outer disk (see Figure 2).

### 3.3. C/N/O Ratios in Dynamic Disks

Here we use the model of Section 2 to estimate the movement of the CO and  $\text{N}_2$  snowlines for different grain morphologies in a viscous disk. Figure 4 shows the  $\text{H}_2\text{O}$ ,  $\text{CO}_2$  and CO snowline locations for particles with initial sizes  $\sim 0.06 \text{ cm} \lesssim s \lesssim 7 \text{ m}$  as well as estimates for the C/O ratio in gas and dust in a viscous disk, with the CO snowline calculated under different grain morphologies as noted above. The true snowline for particles that desorb outside the static snowline is the static snowline itself, hence desorbing particles with  $s < 0.06 \text{ cm}$  do not form true snowlines. If the CO binding environment is known, the CO snowline moves inward by up to  $\sim 50\%$  compared to a static disk for each case (pure and water dominated ices) due to disk dynamics. The full range of potential CO snowlines taking into account both ice morphology and disk dynamics span  $\sim 8.7 \text{ AU}$  to  $\sim 61 \text{ AU}$ , which is a factor of  $\sim 7$  difference. This implies that gas phase C/O ratios of order unity may be reached in the giant planet forming zone, and the CO snowline may be inside 10 AU for certain disk parameters.

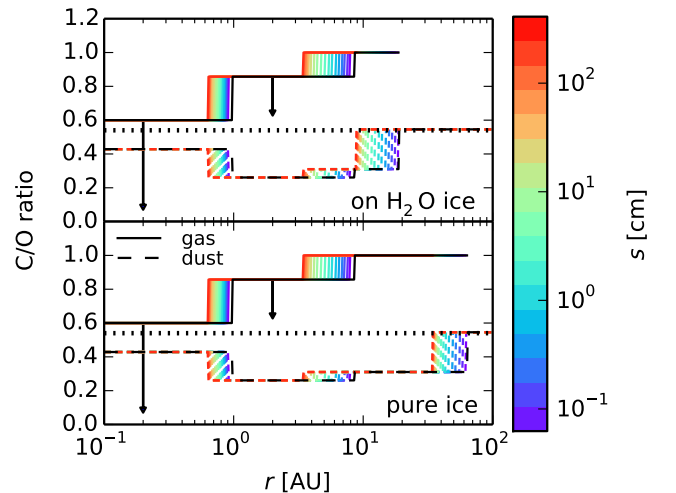


FIG. 4.— C/O ratio estimates in gas (solid lines) and dust (dashed lines) as function of semimajor axis in a viscous disk, for CO residing in a water ice environment (top panel) or as pure CO ice (bottom panel). The  $\text{H}_2\text{O}$ ,  $\text{CO}_2$  and CO snowlines are shown for particles with initial sizes  $\sim 0.001 \text{ cm} \lesssim s \lesssim 7 \text{ m}$  as indicated by the color bar. The C/O ratio in a static disk (black lines) is shown for comparison. The arrows show that the C/O ratio in gas will decrease inside the  $\text{H}_2\text{O}$  and  $\text{CO}_2$  snowlines in the viscous disk, as the relative fluxes of the desorbed icy particles and the overall nebular gas will cause an excess of oxygen gas inside these snowlines (see Paper I for details). Radial drift and gas accretion move the snowlines inward by 40-60%. The presence of CO in a water ice environment rather than as pure ice moves the CO snowline significantly inward by  $\sim 70\%$ .

Figure 5 shows the  $\text{H}_2\text{O}$ ,  $\text{CO}_2$ , CO and  $\text{N}_2$  snowline locations in a viscous disk for the same range of initial particle sizes as in Figure 4, and with the CO and  $\text{N}_2$  snowlines calculated assuming different grain morphologies as explained above, as well as estimates for the N/O



ratio throughout the disk. For simplicity, we assume that all nitrogen is bound in  $N_2$ . This choice is justified since the presence of some  $NH_3$  only moderately changes the N/O ratio (see Figure 3), and since we are primarily interested in the  $N_2$  snowline locations rather than exact values for the N/O ratio. The innermost  $N_2$  snowlines in the viscous disk, created by particles with  $s \sim 7$  m for our fiducial model, are located at  $r_{N_2, \text{pure}} \approx 42$  AU for  $N_2$  as pure ice and at  $r_{N_2, \text{water}} \approx 11$  AU for  $N_2$  in water dominated ices. Thus for each case (pure versus water dominated ices), the  $N_2$  snowline moves inward by up to 50% due to disk dynamics. By taking into account both ice morphology and disk dynamics, the full range of potential  $N_2$  snowlines span  $\sim 11$  to  $\sim 79$  AU, which is a factor of  $\sim 7$  difference. Similarly to the case for CO, the  $N_2$  snowline may be close to or inward of 10 AU for certain disk models.

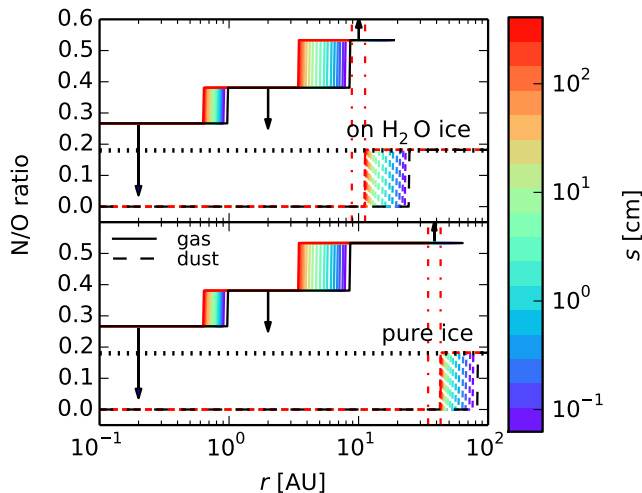


FIG. 5.— N/O ratio estimates in gas (solid lines) and dust (dashed lines) as function of semimajor axis in a viscous disk, for CO and  $N_2$  residing in a water ice environment (top panel) or as pure ices (bottom panel). The  $H_2O$ ,  $CO_2$ , CO and  $N_2$  snowlines are shown for particles with initial sizes  $\sim 0.001 \text{ cm} \lesssim s \lesssim 7 \text{ m}$  as indicated by the color bar. The N/O ratio in a static disk (black lines) is shown for comparison. The arrows show that the N/O ratio in gas will decrease inside the  $H_2O$  and  $CO_2$  snowlines in the viscous disk, as the relative fluxes of the desorbed icy particles and the overall nebular gas will cause an excess of oxygen gas inside these snowlines (see Paper I for details). Radial drift and gas accretion move the  $N_2$  snowline inward by up to  $\sim 50\%$  compared to a static disk. The presence of  $N_2$  in a water ice environment rather than as pure ice moves the  $N_2$  snowline significantly inward by  $\sim 70\%$ . The results of highly enhanced gas-phase N/O ratios in the outer disk compared to its average value, and of highly elevated N/O ratios in gas between the CO and  $N_2$  snowlines (see Figure 3), are preserved.

#### 4. DISCUSSION

#### 5. SUMMARY

In this paper we explore the role of icy grain morphology and disk dynamics on the snowline locations of major volatile carrier molecules and the C/N/O ratios in protoplanetary disks. We enhance the coupled drift-desorption model developed in Piso et al. (2015) by adding more carbon- and nitrogen-bearing species into our framework and by considering different environments in which the icy grains reside. Our results can be summarized as follows:

1. Due to the high volatility of  $N_2$ , the gaseous N/O ratio in the outer disk is enhanced by more than a factor of three compared to its average value. This enhancement is more pronounced than in the case of the gas-phase C/O ratio, which is increased by a factor of two compared to the stellar value. Moreover, the N/O ratio in gas is expected to be very large between the CO and  $N_2$  snowlines due to the complete depletion of oxygen gas in this region.
2. The presence of some carbon in the form of  $CH_4$  and of some nitrogen in the form of  $NH_3$  only modestly affects our results for the C/O and N/O ratios, respectively. In both cases, large C/O and N/O ratios in the outer disk are preserved.
3. Grain composition sensitively affects the CO and  $N_2$  snowline locations. If CO and  $N_2$  are water dominated rather than pure ices, their snowlines move inward by up to  $\sim 70\%$ . This effect is separate from that of radial drift and viscous gas accretion, which also cause an inward movement of the CO and  $N_2$  snowlines by up to  $\sim 50\%$ .
4. The locations of the CO and  $N_2$  snowlines are uncertain when we consider both viscous versus static disks, and pure versus water dominated ices. The snowlines in a viscous disk with CO or  $N_2$  in a water environment are by up to a factor of  $\sim 7$  closer to the host star than in a static disk with CO or  $N_2$  as pure ices.

Our results have direct consequences for the composition of nascent giant planets. The considerable inward movement of the CO and  $N_2$  snowlines due to the ice grains residing in a water ice environment rather than as pure ices implies that giant planets with high C/O and/or N/O ratios in their atmospheres may form closer in than previously predicted by theoretical models. Moreover, our model shows that wide separation gas giants may have an excess of nitrogen in their envelopes, which may be used to trace their origins. In future work, we plan to add new levels of complexity to our model in terms of disk chemistry, dynamics, and planetary dynamics, thus forming a solid framework for understanding the origins of gas giants.

#### REFERENCES

- Ali-Dib, M., Mousis, O., Petit, J.-M., & Lunine, J. I. 2014, *ApJ*, 785, 125  
 Andrews, S. M., Wilner, D. J., Hughes, A. M., Qi, C., & Dullemond, C. P. 2010, *ApJ*, 723, 1241  
 Bergin, E. A., Blake, G. A., Ciesla, F., Hirschmann, M. M., & Li, J. 2015, *Proceedings of the National Academy of Science*, 112, 8965  
 Birnstiel, T., Klahr, H., & Ercolano, B. 2012, *A&A*, 539, A148  
 Bisschop, S. E., Fraser, H. J., Öberg, K. I., van Dishoeck, E. F., & Schlemmer, S. 2006, *A&A*, 449, 1297

- Bottinelli, S., Boogert, A. C. A., Bouwman, J., et al. 2010, *ApJ*, 718, 1100
- Chambers, J. E. 2009, *ApJ*, 705, 1206
- Chiang, E., & Youdin, A. N. 2010, *Annual Review of Earth and Planetary Sciences*, 38, 493
- Collings, M. P., Anderson, M. A., Chen, R., et al. 2004, *MNRAS*, 354, 1133
- Collings, M. P., Dever, J. W., Fraser, H. J., & McCoustra, M. R. S. 2003, *Ap&SS*, 285, 633
- Cruikshank, D. P., Roush, T. L., Owen, T. C., et al. 1993, *Science*, 261, 742
- Evans, II, N. J., Allen, L. E., Blake, G. A., et al. 2003, *PASP*, 115, 965
- Fayolle, E. C., Balfe, J., Loomis, R., et al. 2016, *ApJ*, 816, L28
- Fraser, H. J., Collings, M. P., McCoustra, M. R. S., & Williams, D. A. 2001, *MNRAS*, 327, 1165
- Garrod, R. T., & Herbst, E. 2006, *A&A*, 457, 927
- Henning, T., & Semenov, D. 2013, *Chemical Reviews*, 113, 9016
- Hollenbach, D., Kaufman, M. J., Bergin, E. A., & Melnick, G. J. 2009, *ApJ*, 690, 1497
- Kennedy, G. M., Kenyon, S. J., & Bromley, B. C. 2006, *ApJ*, 650, L139
- Lodders, K. 2003, *ApJ*, 591, 1220
- Madhusudhan, N., Amin, M. A., & Kennedy, G. M. 2014, *ApJ*, 794, L12
- Mandell, A. M., Bast, J., van Dishoeck, E. F., et al. 2012, *ApJ*, 747, 92
- Martín-Doménech, R., Muñoz Caro, G. M., Bueno, J., & Goesmann, F. 2014, *A&A*, 564, A8
- Mollière, P., van Boekel, R., Dullemond, C., Henning, T., & Mordasini, C. 2015, *ApJ*, 813, 47
- Mousis, O., Fletcher, L. N., Lebreton, J.-P., et al. 2014, *Planet. Space Sci.*, 104, 29
- Mumma, M. J., & Charnley, S. B. 2011, *ARA&A*, 49, 471
- Mumma, M. J., Disanti, M. A., dello Russo, N., et al. 1996, *Science*, 272, 1310
- Öberg, K. I., Boogert, A. C. A., Pontoppidan, K. M., et al. 2008, *ApJ*, 678, 1032
- . 2011a, *ApJ*, 740, 109
- Öberg, K. I., Murray-Clay, R., & Bergin, E. A. 2011b, *ApJ*, 743, L16
- Öberg, K. I., van Broekhuizen, F., Fraser, H. J., et al. 2005, *ApJ*, 621, L33
- Owen, T., Mahaffy, P. R., Niemann, H. B., Atreya, S., & Wong, M. 2001, *ApJ*, 553, L77
- Owen, T. C., Roush, T. L., Cruikshank, D. P., et al. 1993, *Science*, 261, 745
- Pérez, L. M., Carpenter, J. M., Chandler, C. J., et al. 2012, *ApJ*, 760, L17
- Piso, A.-M. A., Öberg, K. I., Birnstiel, T., & Murray-Clay, R. A. 2015, *ApJ*, 815, 109
- Pontoppidan, K. M. 2006, *A&A*, 453, L47
- Qi, C., Öberg, K. I., Wilner, D. J., et al. 2013, *Science*, 341, 630
- Rodgers, S. D., & Charnley, S. B. 2002, *MNRAS*, 330, 660
- Rubin, M., Altwegg, K., Balsiger, H., et al. 2015, *Science*, 348, 232
- Shakura, N. I., & Sunyaev, R. A. 1973, *A&A*, 24, 337
- Wyckoff, S., Tegler, S. C., & Engel, L. 1991, *ApJ*, 367, 641
- Zhang, K., Pontoppidan, K. M., Salyk, C., & Blake, G. A. 2013, *ApJ*, 766, 82